The X-ray shadow in the south-east of the Large Magellanic Cloud

M.J. Blondiau, J. Kerp, U. Mebold, and U. Klein

Radioastronomisches Institut der Universität Bonn, Auf dem Hügel 71, D- 53121 Bonn, Germany

Abstract. We analyze mosaiked *ROSAT* PSPC pointings towards the Large Magellanic Cloud (LMC). Focussing on the area south-east of 30 Doradus roughly at the position of RA(2000) = 5^h40^m and DEC(2000) = $-70°$, we verify the existence of an X-ray absorption feature. The *ROSAT* data imply that X-ray attenuating material is located in front of a diffuse X-ray source that extends from the eastern boundary of the LMC to west of the giant molecular cloud south of 30 Dor. The difference of the absorbing hydrogen column densities, derived from the *ROSAT* data, between the X-ray bright "wedge" region and dark "shadow" region is about $N_H = (7.0 \pm 1.8) \cdot 10^{21}$ cm^{-2}. This column density difference is consistent with the value derived from *IRAS* 100 μm emission map of this region which leads to total hydrogen column densities of $N_{Wedge} = (5.2 \pm 0.9) \cdot 10^{21}$ cm^{-2} towards the X-ray bright and $N_{Shadow} = (11.1 \pm 2.2) \cdot 10^{21}$ cm^{-2} towards the X-ray dark regions. The agreement between these values derived from the *ROSAT* and *IRAS* data suggest that a part of the extended diffuse X-ray emission is located on the far side of the giant molecular cloud.

This kind of 3-D structure is independently verified by radio continuum observations. The X-ray attenuating gas is positionally associated with the polarized radio continuum emission of a giant magnetic loop emerging out of the plane of the LMC. Faraday depolarization implies that this magnetized loop penetrates deep into - or beyond - the LMC, possibly commencing in the X-ray emitting plasma of the LMC.

Key words: galaxies: ISM; Magellanic Clouds – ISM: structure – X-rays: ISM – diffuse radiation

1. Introduction

Trümper et al. (1991) and Wang et al. (1991) verified the existence of widely distributed hot gas in the LMC. They derived plasma temperatures ranging from $10^{6.4}$ to 10^7 K. This discovery suggests a large energy input into the interstellar medium (ISM) of the LMC and implies that the starforming regions play

Send offprint requests to: M.J. Blondiau

an important role in the evolution of the LMC gas component. The *ROSAT* X-ray satellite (Trümper et al. 1983), in combination with the position sensitive proportional counter (PSPC; Pfeffermann et al. 1986) provides an angular and spectral resolution which permits a deep insight into the distribution of the hot phase of the ISM of the LMC. Snowden & Petre (1994) showed that the X-ray emission across the whole LMC cannot be explained by the emission of a single temperature plasma, because of their detection of a steep X-ray energy gradient across the "bar" of the LMC.

In this paper we present a solution of the X-ray radiative transfer equation through the neutral gas in the eastern part of the LMC. In Sect. 2 we present our data. In Sect. 3 we discuss the X-ray radiation transfer equation and present a 3-D model of X-ray emitting and absorbing layers. In Sect. 4, we compare our results with the distribution of the polarized radio continuum emission in the LMC, which corroborates our 3-D X-ray emission and absorption model. Sect. 5 summarizes our results and discusses some implications.

2. Observations and data reduction

We have analyzed pointed *ROSAT* X-ray data of the LMC extracted from the *ROSAT* public data archive. The area of interest includes 30 Dor and the molecular cloud region south of it. The whole area is covered by 81 individual pointed PSPC observations which were observed from 16 June 1990 to 24 September 1993. A maximum integration time of about 204.5 ksec can be analyzed. The final map, presented in Fig. 1, is centred at RA(2000) = $5^h40^m4^s.8$ and DEC(2000) = $-70°13'48''$.

2.1. Data processing

Pointed *ROSAT* PSPC data have to be corrected for various effects associated with the so-called non-cosmic X-ray backgrounds (Snowden et al. 1994). The strongest X-ray background contribution can be attributed to scattered solar X-rays (Snowden & Freyberg 1993) and short-term enhancements. Their effects are directly visible by studying the variation of count rates versus observing time. In accord with the data processing procedure described by Kerp (1994) we selected time intervals of the individual observing periods which show no deviation from
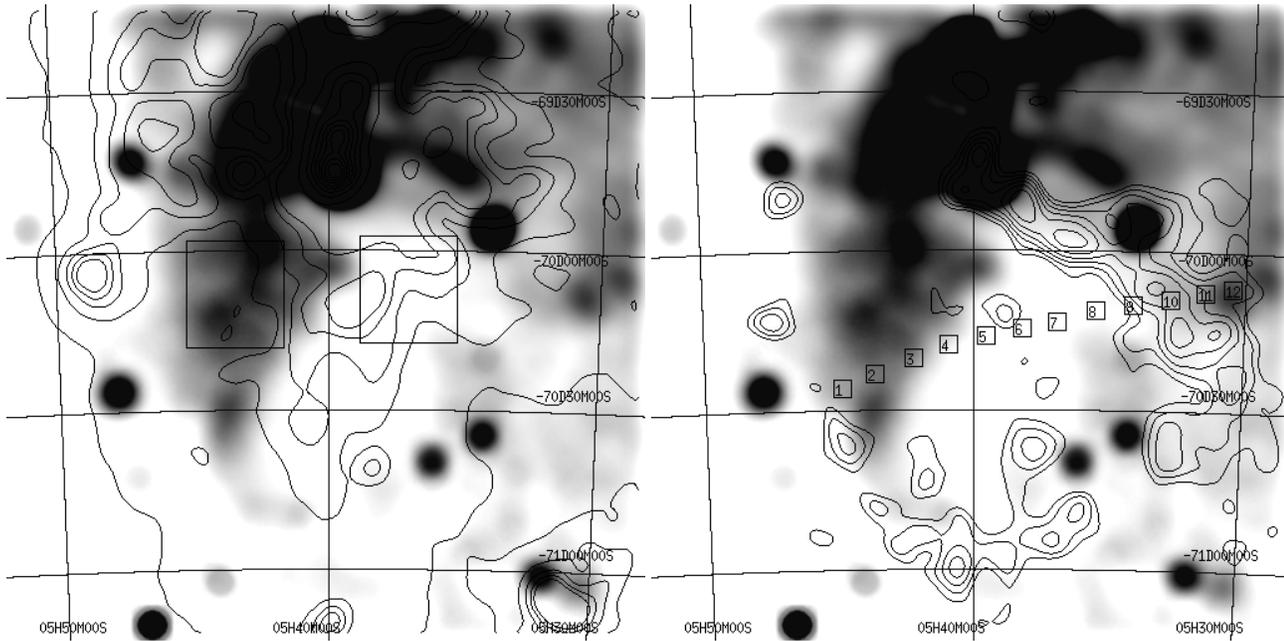
Fig. 1. The grey-scale maps represent the *ROSAT* R4–R7 band brightness distribution of the area south of 30 Dor. The X-ray bright region of diffuse X-ray emission is called "wedge" in this *paper* due to its shape. The X-ray dark region on the western side of the wedge is the X-ray "shadow". The logarithmic intensity scale ranges from $5 \cdot 10^{-4}$ to $20 \cdot 10^{-4}$ counts s^{-1}arcmin^{-2}. The maps have been smoothed to an angular resolution of $4'$. Left: The *IRAS* 100 μm intensity distribution is superimposed as contours, the contour levels are 2 to 10% in steps of 2% and 10 to 100% in steps of 10% of the maximum. The maximum intensity is localized in the northern part of the map (920 MJy sr^{-1}). The *IRAS* map has an angular resolution of about $2'$. Right: The contour lines represent the 6.3 cm polarized radio continuum intensity (Klein et al. 1993). The contour levels range from 40 to 100% in steps of 10% of the maximum value, which is 68 mJy/b.a. The angular resolution of the map is $4'.5$. The superimposed boxes mark the areas in which we analyse the X-ray spectra (Fig. 5).

Table 1. Measures of the average column densities in the boxes defined in Fig. 1. H I column densities are taken from Luks & Rohlfs (1992). The values for the CO line integral are taken from the map published by Cohen et al. (1988).

REGION	N_H fitted 10^{21} cm^{-2}	N_{HI} total 10^{21} cm^{-2}	*IRAS* $I_{100\mu m}$ MJy sr^{-1}	*IRAS* $I_{60\mu m}$ MJy sr^{-1}	N_H from $I_{100\mu m}$ 10^{21} cm^{-2}	W_{CO} K km s^{-1}	X_{WCO} 10^{21} H$_2$ (K km s^{-1})$^{-1}$
WEDGE	6.9±0.2	3.92±0.1	31.13	9.09	5.2±0.9	1.6±0.2	0.4±0.3
SHADOW	13.9±1.6	3.92±0.1	66.56	24.35	11.1±2.0	1.9±0.2	1.9±0.6

the minimum count rate measured over the whole observing period. The LMC X-ray brightness distribution reveals its full complexity at photon energies above 0.5 keV (Snowden & Petre 1994). This photon energy corresponds to a plasma temperature $\geq 10^{6.5}$ K, which is significantly hotter than the X-ray plasma of the solar corona (Snowden & Freyberg 1993). Thus, the contamination of the X-ray data by scattered solar X-rays decreases with increasing photon energy. The application of the time selection method of Kerp (1994) limits the data strongly in observing time because it selects primarily for night-side periods of the *ROSAT* orbit. During the night-side of the *ROSAT* orbit, the influence of scattered solar X-ray reaches a minimum. At higher X-ray energies the data are increasingly affected by particle background events. We followed the procedure described by Plucinsky et al. (1993) and calculated the contribution of

the particle background to the data and subtracted it. The X-ray data were cast into the standard *ROSAT* energy bands defined by Snowden et al. (1994). By mosaiking of the exposure-map-corrected X-ray data, we produce final images of the whole LMC.

The influence of the long-term enhancements can be monitored by the mapping procedure (compare Fig. 2). The large positional overlap of the individual PSPC pointings, which are observed at different times, directly reveals significant variations of the absolute X-ray background intensity level. Fig. 3 shows the "light curve" of the area of interest (wedge) in the R4 band, which is most affected by the long-term enhancements of all analysed *ROSAT* energy bands. The different PSPC observations contributing to the wedge area show over a period of two years comparable count rates within the individual 3σ uncer-
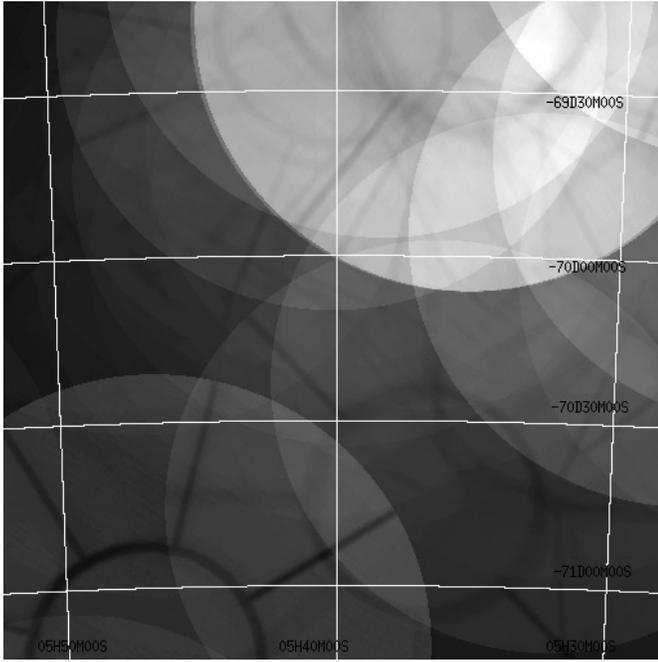
Fig. 2. This figure shows the distribution of the individual *ROSAT* PSPC pointings across the area of interest, indicated by their corresponding exposure maps. The integration time ranges from 0 up to 204.5 ksec with a mean integration time of 66.5 ksec.

tainty levels. This result suggests that the area of interest is not significantly affected by long-term enhancements or residuums of the other non-cosmic background constituents. This gives us the possibility to investigate the X-ray radiative transfer in detail.

Due to the fact that each area of the sky is covered by several pointed observations which were centred at different sky positions no well-defined point-spread function exists. Consequently, for the analysis of the diffuse X-ray emission we reject areas around point sources as large as the largest point-spread function of the PSPC.

In our search for, and analysis of, the X-ray shadow we used different methods. First of all, we derived band ratios of two neighbouring energy bands. Band ratios are very sensitive in verifying the existence of X-ray absorption along the line-of-sight, owing to the strong energy dependence of the photoelectric absorption cross section (Morrison & McCammon 1983).

Secondly, we tried to identify the detected X-ray absorption feature in size and shape with the distribution of tracers of neutral matter like H I , *IRAS* 100 μm, and ^{12}CO(1 $\rightarrow$ 0) data. Finally, we extracted X-ray spectra. These X-ray spectra allow us to evaluate the temperature and emission measure of the X-ray plasma located beyond the absorption feature. The spectra presented in this paper were produced by subtracting an "OFF" spectrum from the spectra of LMC objects. This "off-source" spectrum was determined in an area located at an angular distance of about 1°7 to the south-east of the LMC, roughly at the position of RA(2000) = 6^{h}10^m and DEC(2000) = −71°30′.

3. The X-ray shadow

We have investigated a region located south of 30 Dor (Fig. 1). At X-ray photon energies $\geq$ 0.5 keV, equivalent to the *ROSAT* energy bands R4 and above (Snowden et al. 1994), the complexity of the X-ray structure in the LMC becomes visible. Snowden & Petre (1994) proposed that the X-ray dark area south of 30 Dor is associated with a soft X-ray shadow. As a first quantitative check of this suggestion we have calculated various *ROSAT* energy band ratios. Since the photoelectric absorption cross section decreases with increasing photon energy (Snowden et al. 1994), a hardening of the attenuated X-ray energy spectrum should be detectable. In this case the $\frac{R7}{R6}$ ratio is expected to peak just at the position of the dimmest area. This is indeed what we find within the area close to 30 Dor (see Fig. 4).

The high angular resolution of the *ROSAT* PSPC reveals a rather narrow transition zone between the suspected shadow and the wedge-shaped X-ray emission structure at the eastern boundary of the LMC. We adop as a working hypothesis that the X-ray plasma beyond the shadow and in the wedge is the same, and solve the X-ray radiative transfer equation. This equation has the form:

$$I_{\text{det.}} = I_{\text{LHB}} + I_{\text{gal}} \cdot e^{-\sigma_{\text{gal}} \cdot N_{\text{H gal}}} +$$
$$+ I_{\text{LMC}} \cdot e^{-\sigma_{\text{LMC}} \cdot N_{\text{H LMC}}} \cdot e^{-\sigma_{\text{gal}} \cdot N_{\text{H gal}}} +$$
$$+ I_{\text{cos}} \cdot e^{-\sigma_{\text{LMC}} \cdot N_{\text{H LMC}}} \cdot e^{-\sigma_{\text{gal}} \cdot N_{\text{H gal}}}. \quad (1)$$

Here I_{LHB}, I_{gal}, I_{LMC}, and I_{cos} denote the count rates of a specific energy band orginating from the local hot bubble (LHB, Snowden et al. 1990), the galactic halo, the ISM of the LMC, and the extragalactic background. $N_{\text{H gal}}$ and $N_{\text{H LMC}}$ denote the attenuating column densities of the ISM in the Galaxy and the LMC, respectively, while σ_{gal} and σ_{LMC} denote the corresponding photoelectric cross sections.

This full radiative transfer equation can be simplified by analyzing only the photon events detected at energies above the *ROSAT* R4 band. Here the LHB intensity I_{LHB} can be neglected because its emission is mostly in the R1 and R2 energy bands (Snowden et al. 1993). The I_{gal} term is not restricted to these two soft *ROSAT* energy bands, it contributes significantly up to the R4 band. This can be traced by the fact that the intensity band ratio $\frac{R6}{R5}$ shows a similar behaviour as the ratio $\frac{R7}{R6}$ (see Fig. 4) while the $\frac{R5}{R4}$ ratio of the same slice across the shadow looks completely different. Therefore we can conclude that the R4 band is still influenced by a softer X-ray plasma like I_{gal} but the R5 band is not any longer significantly affected by the contribution of the galactic X-ray plasma. The amount of attenuating galactic H I column density is more than an order of magnitude lower than the amount of neutral matter associated with the LMC itself, moreover it is smoothly distributed across the analysed area. Therefore its contribution to the X-ray absorption feature can be neglegted in the radiation transport equation by analysing count rate differences and ratios. Thus the radiative transfer equation for the harder part of the *ROSAT* X-ray range ($E \geq$ R5) has the form:

$$I_{\text{det.}} \simeq (I_{\text{LMC}} + I_{\text{cos}}) \cdot e^{-\sigma_{\text{LMC}} \cdot N_{\text{H LMC}}} \cdot e^{-\sigma_{\text{gal}} \cdot N_{\text{H gal}}}. \quad (2)$$
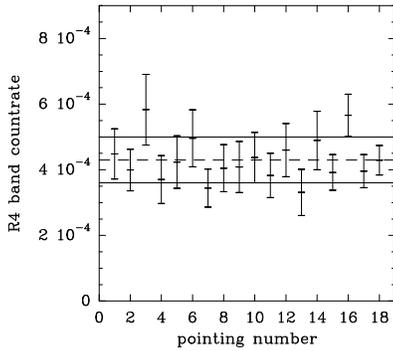
Fig. 3. This figure shows the R4 band count rates of 18 *ROSAT* PSPC pointings averaged across the box area towards the X-ray wedge (Fig. 1). The count rates are weighted according to their area coverage to the box area for each pointing. Over a time period of roughly two years all pointings reveal comparable count rates within the individual 3σ uncertainty levels. The dashed line indicates the mean value of all R4 band count rates. The solid lines show the 1σ deviation from the mean value. We therefore conclude that the contribution of the so called long-term X-ray enhancements is insignificant in the area under investigation.

In the following we will use the abbreviations N_S and N_W for the total column densities N_{Shadow} and N_{Wedge}, and I_S and I_W for I_{Shadow} and I_{Wedge}. I_{bS} and I_{bW} denote the intensities originating beyond the absorbing matter towards both areas. In order to evaluate the difference $\Delta N(Ri) = N_S - N_W$ (i = 5,6,7) of the absorbing column densities towards the shadow and the wedge we can write:

$$I_S(Ri)/I_W(Ri) \simeq I_{bS}(Ri)/I_{bW}(Ri) \cdot e^{-\sigma(Ri,\overline{N})\cdot(N_S - N_W)} \quad (3)$$

assuming that the brightness of the diffuse X-ray emission of the LMC behind the wedge and the shadow is constant ($I_{bS} = I_{bW}$). This is also valid for the contribution of the extragalactic component consisting of unresolved point sources (Hasinger et al. 1993). This assumption is supported by the rather steep intensity contrast between wedge and shadow on small angular scales, and will be substantiated further by the agreement of the column densities derived here and the values derived from the *IRAS* $100\,\mu$m intensities (see below). Evaluating Eq.(3) we find $\Delta\overline{N} = \overline{N}_S - \overline{N}_W = (4.4 \pm 0.6) \cdot 10^{21}\,\text{cm}^{-2}$. Thus, as a first result, we can conclude that the X-ray contrast between the wedge and shadow area is associated with a difference in absorbing column density of $\Delta\overline{N} \simeq 4.4 \cdot 10^{21}\,\text{cm}^{-2}$.

Next we will check whether or not ΔN is consistent with the values derived from secondary tracers of the neutral matter. First, we estimate the column densities of the atomic neutral hydrogen in the areas of interest. The values given in Table 1 (column "N_{HI} total") are averaged across the two boxes located at the wedge and the shadow (see Fig. 1). They were derived from the H I data of Luks & Rohlfs (1992) after rescaling their brightness temperature calibration upwards by a factor of 1.5 (Osterberg 1996). Obviously the derived H I column density difference between the wedge and shadow area cannot account

for the apparent X-ray shadow. Thus, the neutral atomic hydrogen is not the dominant absorbing agent along the line-of-sight towards the shadow.

Second, we consider the *IRAS* $100\,\mu$m intensity distribution, because this will give us an estimate of both, the atomic and the molecular constituent of the absorbing hydrogen column density (Herbstmeier et al. 1993). Comparing the $100\,\mu$m intensities of the wedge and the shadow (Table 1) indeed shows that the X-ray intensity contrast is compatible with the contrast of the $100\,\mu$m *IRAS* emission. Converting $I_{100\,\mu m}$ to N_{HI} by a factor of $0.6\,\text{MJy sr}^{-1} \cdot 10^{-20}\,\text{cm}^2$ (Schwering 1988, Osterberg 1996) the total absorbing column density at the position of the wedge becomes $N_W = (5.2 \pm 0.9) \cdot 10^{21}\,\text{cm}^{-2}$ and on the shadow $N_S = (11.1 \pm 2.0) \cdot 10^{21}\,\text{cm}^{-2}$. In order to make sure that the infrared intensity difference is not caused by any spatial variation of dust temperatures we have studied the ratio of the intensities at $100\,\mu$m and $60\,\mu$m in the area of the wedge and the shadow. We find this ratio to be constant across the area of interest, indicating that the *IRAS* intensity differences are associated with column density variations. It is satisfying to see that the column density difference $\Delta N = (5.9 \pm 2.2) \cdot 10^{21}\,\text{cm}^{-2}$ derived from the *IRAS* $100\,\mu$m intensities agrees, within the uncertainties, with the value derived from the X-ray data. This justifies the assumption of a constant X-ray background intensity beyond the wedge and the shadow. It suggests that X-ray emission associated with the LMC is located beyond most, or all of the X-ray absorbing material.

Finally in our analysis of *ROSAT* data, we have used X-ray spectra to analyze the extended X-ray background behind the wedge and the shadow (see Fig. 5). First, we extracted an X-ray spectrum for the wedge-shaped X-ray bright emission region averaged over the area marked in Fig. 1. We then subtracted a background spectrum sampled at a position "OFF" the LMC. This is necessary because there is a significant contribution of the galactic X-ray plasma in the R4 band. This component shows up in the $\frac{R5}{R4}$ ratio: In case of a pure absorption feature this ratio is expected to peak like the $\frac{R6}{R6}$ and $\frac{R7}{R6}$ ratios (compare Fig. 4). But what we detect is a local minimum of the $\frac{R5}{R4}$ ratio just at the same position where the other ratios reaches local maxima. Furthermore, if we do not substract the background spectrum the fit becomes worse. On the other hand this substraction leads to an additional source of uncertainty. At the "OFF" position a nearly unabsorbed extragalactic radiation spectrum is determined while towards the wedge and shadow the extragalactic background radiation is absorbed by the whole X-ray attenuating column density of the LMC. To account for this difference in absorbing column density between the "OFF" position and both areas of interest we evaluated, according to Hasinger et al. (1993), the contribution of the extragalactic background to both X-ray spectra. As a dotted line we indicate the absolute extragalactic background level in Fig. 5. Obviously, towards the wedge area the contribution of the extragalactic background radiation to the observed X-ray intensity is insignificant. Towards the shadow its contribution is only a factor of 4 below the observed X-ray intensities. Thus, the performed subtraction of the "OFF" LMC
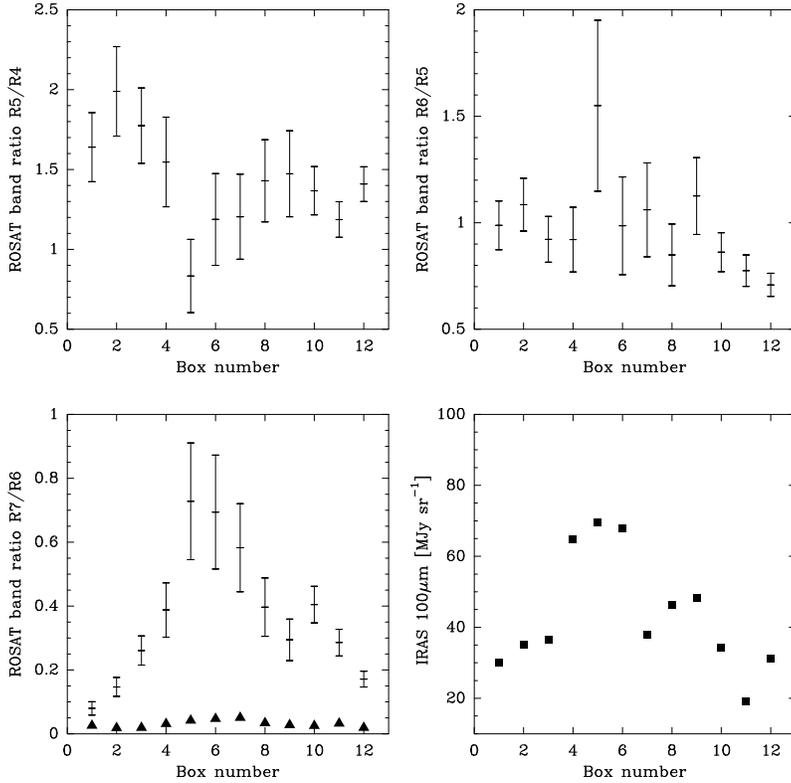
Fig. 4. The *ROSAT* energy band ratios $\frac{R5}{R4}$, $\frac{R6}{R5}$ and $\frac{R7}{R6}$ as a function of position across the area of interest. For comparison the right-hand diagram at the bottom shows the *IRAS* 100 μm intensity as a function of the same positions. For the location of the individual boxes and their corresponding numbers, examine the right-hand side of Fig. 1. The boxes 5 to 9 cover the X-ray dark area. The triangles indicate quantitatively the contribution of the extragalactic X-ray background radiation determined from the parametrization of Hasinger et al. (1993) to the observed $\frac{R7}{R6}$ band ratio. Obviously, its contribution is small compared to the $\frac{R7}{R6}$ ratio amplitude variation detected. In particular it does not alter the characteristic shape of the count rate ratio with the position across the shadow. For the other band ratios the contribution of the extragalactic component is even smaller.

background spectrum is an overcorrection for the shadow area. However, the X-ray spectrum of the shadow shou ld not stressed too much, because of the strong statistical limitation of the X-ray data (compare the size of the corresponding error-bars in Fig. 5). In fitting a Raymond & Smith (1977) plasma model to the X-ray spectrum of the wedge we adopted a reduced metallicity (0.5 dex; see e.g., Westerlund 1990) and fixed the absorbing column density to the value derived from $I_{100\,\mu m}$. The highly significant fit for the spectrum on the wedge yields an unabsorbed X-ray flux of $(2.2 \pm 0.1) \cdot 10^{-13}$ erg cm^{-2} s^{-1} arcmin^{-2} in the *ROSAT* energy range $E = 0.1 - 2.4$ keV. The derived plasma temperature is $T = 10^{6.5 \pm 0.1}$ K, with an emission measure of $EM(\text{wedge}) = 1.0 \pm 0.7$ cm^{-6} pc. As a final check for consistency we derive an estimate of the column density on the shadow by fitting the thermal plasma, fixed in emissivity and temperature to the values derived from the wedge, with the attenuating column density as the single free parameter of the fit. Towards the shadow this spectral fit gave an attenuating column density of $N_S = (13.5 \pm 0.8) \cdot 10^{21}$ cm^{-2}. Taking into account the low statistical significance of the shadow X-ray spectrum, the derived column density value is comparable to the value derived from the *IRAS* data (Table 1). However, the X-ray spectrum of the shadow shows the strong attenuation of the X-ray background radiation towards the high column density regions of the LMC.

In order to obtain a deeper insight into the chemical composition of the X-ray absorbing medium we will separate the atomic and molecular hydrogen content. A quantitative comparison of the H I column densities, the column densities de-

rived from *IRAS* 100 μm emission and that determined from the X-ray absorption allows an estimate of the molecular hydrogen column densities. These in turn can be compared with available data on the line integral W_{CO} [K km s^{-1}] of the $J = 1 \rightarrow 0$ transition of the ^{12}CO molecule, thus obtaining a new and independent measure of the frequently discussed X_{WCO} factor. This factor is often used to derive molecular hydrogen column densities N_{H_2} [cm^{-2}] from the equation:

$$N_{H_2} = X_{WCO} \times W_{CO}. \qquad (4)$$

For the wedge, the total column density is larger than the H I content by a factor of $(1.3 \pm 0.9) \cdot 10^{21}$ cm^{-2}. Assuming that $I_{100\,\mu m}$ is proportional to the sum of the number of hydrogen atoms and twice the number of hydrogen molecules, the molecular hydrogen column density for the wedge is about $N_{H_2} = (0.6 \pm 0.4) \cdot 10^{21}$ cm^{-2}. For the shadow we get $N_{H_2} = (3.6 \pm 1.0) \cdot 10^{21}$ cm^{-2}. In conjunction with the ^{12}CO data of Cohen et al. (1988) (see Table 1, Column 6) we obtain X_{WCO} factors of about $(0.4 \pm 0.3) \cdot 10^{21}$ H$_2$ (K km s^{-1})$^{-1}$ for the wedge and $(1.9 \pm 0.6) \cdot 10^{21}$ H$_2$ (K km s^{-1})$^{-1}$ for the shadow. While the average of the two values is in agreement with the X_{WCO} factor derived by Cohen et al. (1988), the individual values are rather discrepant. The more detailed distribution of W_{CO} obtained in the ESO key project (Kutner 1996) shows a rather narrow ^{12}CO filament extending in a north-south direction along the boundary between wedge and shadow. This suggests that W_{CO} [K km s^{-1}] is not a measure of column density but is dominated by excitation effects.

The determination of the differential 3-D structure of X-ray absorbing and emitting layers in the LMC reveals the power of
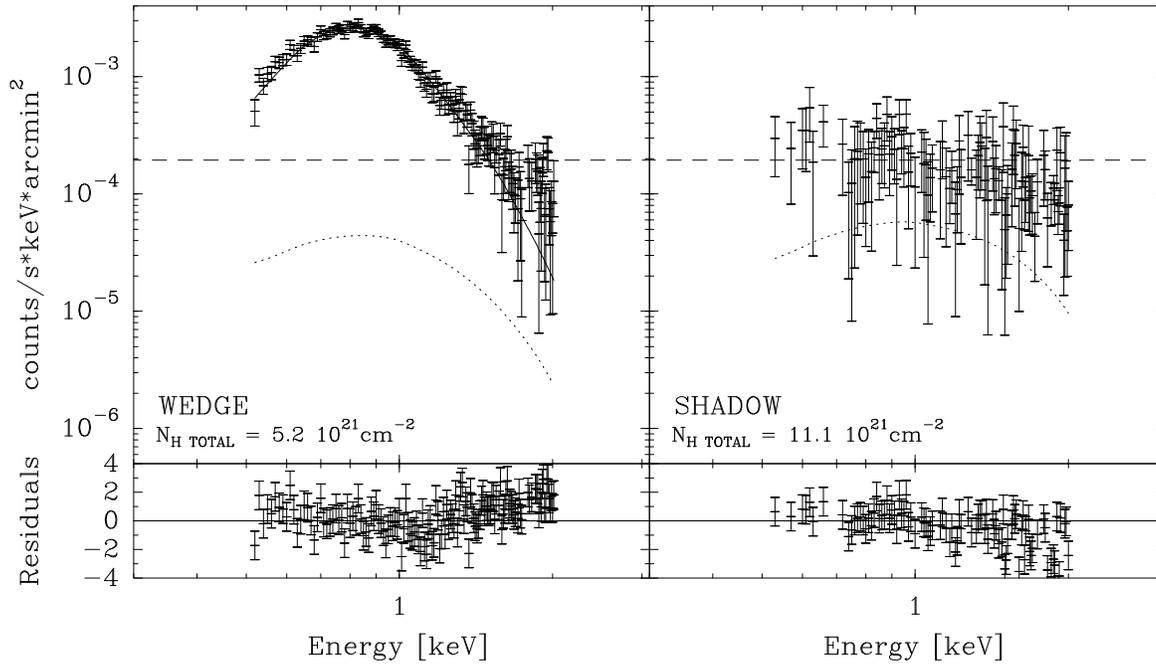
Fig. 5. X-ray spectra obtained in the box areas marked on the left-hand side of Fig. 1. The left-hand side displays the spectrum of the wedge-shaped structure of enhanced diffuse X-ray emission, while the right-hand diagram shows that of the shadow. A background spectrum has been subtracted which was obtained from a *ROSAT* pointing located about 1°7 to the east of the map centre of Fig. 1. We have fitted a Raymond & Smith (1977) plasma model with a reduced metallicity of about 0.5 dex to the observed data. The fits and residuals are also displayed. The dotted curves show the shape of a possible "overcorrection" term which is caused by substracting an already unabsorbed extragalactic spectrum. This "overcorrection" is derived from a spectral power law model for the contribution of unresolved extragalactic sources (Hasinger et al. 1993). At least at the position of the wedge an overcorrection does not affect the shape of the LMC intrinsic spectrum significantly. The dashed line is the mean value of the spectral data in the area of the shadow.

the analysis of X-ray data of extended extragalactic sources in general. An independent confirmation of the 3-D structure derived above is provided by radio continuum polarization results.

4. The magnetic loop south of 30 Dor

On the right-hand side of Fig. 1 we show an X–ray map superimposed by contours of the 6.3 cm linearly polarized radio continuum emission. The polarized emission of the LMC at 21, 12, and 6.3 cm was measured by Haynes et al. (1993) and further investigated by Klein et al. (1993). The maximum emission in the two polarized filaments changes its location towards the south-west in the northern and towards the west in the southern filament with increasing wavelength. Analysis of Faraday rotation and depolarization led Klein et al. (1993) to conclude that the best explanation of the polarization structure is in terms of a giant magnetic loop emerging out of the plane of the LMC.

Since Faraday rotation is proportional to λ^2, and depolarization can depend even more strongly on wavelength, the line-of-sight of the polarized radiation penetrates deepest into the magneto-ionic medium at 6.3 cm. At this wavelength the northern filament has its brightest emission at the northern edge of the deep X-ray shadow, where it ends near the bright X-ray source LMC X-1. Towards the south the filament can be traced to the tip of the wedge-shaped X-ray emission region in the southern part

of the X-ray shadow. Hence, it appears as if the X-ray shadow is located within the magnetic loop, and it is where the loop seems to end deep in the gas that the wedge-shaped structure of enhanced X-ray emission commences. One is therefore led to conclude that the magnetic loop closes somewhere inside or behind the region of the bright diffuse X-ray emission.

This positional association can be used to sketch a 3-D scenario of the LMC at its eastern interface to the Galactic halo. The polarization observations have been used to derive rotation measures, RM, for the plasma located between the polarized radio loop and the observer. About 1° to the south-west of the northern end of the loop Klein et al. (1993) derived RM = 40 rad m^{-2}. This can be used to estimate the density of thermal electrons from the equation

$$\text{RM} = 0.812 \cdot \int \frac{n_{\text{e}}}{\text{cm}^{-3}} \cdot \frac{B_{\parallel}}{\mu\text{G}} \cdot \frac{ds}{\text{pc}} \quad \text{rad m}^{-2}. \tag{5}$$

Adopting the component of the magnetic field along the line-of-sight to be $B_{\parallel} \sim 2~\mu\text{G}$ (Klein et al. 1993) and estimating the length of the line-of-sight through the magneto-ionic medium from the diameter of the northern filament to be about 440 pc ($\sim$ 30′) we find a density of thermal electrons of $n_{\text{e}} \sim 0.06~\text{cm}^{-3}$. This mean electron density refers to a volume located in front of the outer part of the loop which was found to be emerging out of depolarizing material in the LMC.

Similar densities can be inferred for the thermal electrons of the X-ray plasma in the wedge by using the emission measure derived in Sect. 3. We find $n_e = 0.05^{+0.01}_{-0.02}$ cm^{-3}, if the line-of-sight through the X-ray emitting region of the wedge is also ~ 440 pc (see above).

We adopt the hypothesis that these electron densities refer to the same region in the LMC. It then appears that the Faraday rotation in the region of the polarized filaments is produced by the extended hot plasma whose X-ray emission shows up in the east, i.e., in the wedge, and is associated with the material producing the X-ray shadow in the west. This would solve the problem noted by Klein et al. (1993) that the Faraday rotation and the depolarization in this area cannot be reconciled with the thermal electron densities inferred from the thermal free-free radio emission. The thermal emission has to be placed in the background of the polarized loop because it would lead to rotation measures which are clearly larger than what is observed. This corroborates the view that the enhanced X-ray emission is physically related to the magnetic loop, which in turn could be a result of an interaction with the ambient medium at the eastern, i.e., the leading edge of the LMC.

Combining this with the result that the X-ray emission originates behind the bulk of the neutral material in the LMC (see Sect. 3) we arrive at the following scenario: The magnetic loop commences at the far side of the LMC - possibly within the X-ray emitting region that we call the wedge. As already noted by Klein et al. (1993), the magnetic loop stretches between the main disk of the LMC and a sub-structure of the LMC at a relatively low velocity, the so-called "L-component" (Luks & Rohlfs 1992). Then the loop emerges from the ISM of the LMC towards our Galaxy at the western edge of the dark X-ray shadow. This edge coincides very closely with the location of a steep gradient of total H I column density and magellano-centric velocities in the LMC and - not quite as closely - with the western edge of the L-component (Luks & Rohlfs 1992). The observed drop of Faraday rotation in the loop can then be attributed to the emergence of the polarized loop from behind the western edge of the material producing the X-ray shadow.

Trying to associate the material producing the X-ray shadow with the L-component we run into problems - that can be solved. First, the column density inferred from X-ray absorption exceeds by far the H I content of the L-component. It is in fact about twice as large as the H I gas of L- and the "D-component" taken together (see Sect. 3). Second, the increase of Faraday rotation in proceeding from the south-west to the north-east is closely correlated to the total H I column density but only marginally so to that of the L-component. The first problem can be avoided by assuming that most of the molecular hydrogen derived above is associated with the L-component. This is supported by the velocities of the CO lines observed by Cohen et al. (1988) in the LMC. These velocities fall in the range of the characteristic velocities of the L-component (Kampmann 1996, Johansson et al. 1994). The other problem can be solved by revising the separation by Luks & Rohlfs (1992) of the two major H I components of the LMC. A separation that assigns most of the bright H I ridge south of 30 Dor to the L-component would

change the results of Luks & Rohlfs (1992) only insignificantly but would lead to consistency with our findings. More details of such a revision will be published in a forthcoming paper (Blondiau 1996, in prep.).

Independent of the details of such a separation, it appears that the material producing the X-ray shadow is located in front of the LMC disk and is moving away from the disk towards the Galaxy. As the field is probably tied to the gas, the disruption of the L-component from the disk must have dragged the field along, regardless of what kind of mechanism is responsible for this disturbance.

5. Summary and conclusions

We confirm the existence of the X-ray shadow south of 30 Dor in the LMC first reported by Snowden & Petre (1994). *ROSAT* X-ray band ratios imply that the X-ray dark structure in the south-east of 30 Dor that we called the "shadow" is caused by absorption of background X-ray radiation. Solving the X-ray radiative transfer equations valid at photon-energies above 0.5 keV for the shadow and the X-ray bright region east of the shadow – which we called "wedge" – reveals that the shadow is caused by an excess of the equivalent hydrogen column density of $\Delta N \simeq (4.4 \pm 0.6) \cdot 10^{21}$ cm^{-2} between wedge and shadow. Using the *IRAS* 100 μm dust emission as a tracer of attenuating matter along the line-of-sight, we confirm this column density difference within the uncertainties and derive hydrogen column densities of about $N_S = (11.1 \pm 2.2) \cdot 10^{21}$ cm^{-2} in the shadow and $N_W = (5.2 \pm 0.9) \cdot 10^{21}$ cm^{-2} in the wedge. N_W is also consistent with the absorbing column density in front of the X-ray emitting plasma estimated from model fits to the *ROSAT* spectrum observed on the wedge.

From a quantitative comparison of H I 21 cm line column densities and *IRAS* 100 μm data we derive column densities of molecular hydrogen, N_{H_2}. We found insignificant amounts of N_{H_2} in the wedge and a column density of $N_{H_2} = (3.6 \pm 1.0) \cdot 10^{21}$ cm^{-2} in the shadow. In comparison with available information on ^{12}CO emission indicates that there is no unique correlation between the ^{12}CO line integral and the molecular hydrogen column densities.

The X-ray plasma in the wedge appears to have a temperature of $T_{X-ray} \simeq 10^{6.5}$ K and an emission measure of $EM(\text{wedge}) = 1.0 \pm 0.7$ cm^{-6} pc. It is widely distributed over the eastern and the far side surface of the LMC. One can estimate an X-ray luminosity of $L_X \simeq 4.0 \cdot 10^{37}$ erg s^{-1} in the *ROSAT* energy range if one assumes a X-ray emitting volume equivalent to that of a sphere with diameter $d \simeq 440$ pc corresponding to an angular diameter of $\sim 30'$ (see Fig. 1). This diameter is an average value for the extension of the wedge-shaped X-ray emitting structure. Estimating the pressure in this volume from the temperature and the emission measure given above we obtain $n_e \cdot T = 1.5 \cdot 10^5$ K cm^{-3}. This value is more than a factor of 10 larger than typical values for the pressure in our Galaxy (see below). Assuming that the hot gas in the eastern part of the LMC is in pressure equilibrium with the ram pressure, which is possibly created by the movement of the LMC

through the Galactic halo, one can deduce the density of the Galactic halo in the following way: Approximating the LMC as a solid body moving through the hot galactic halo gas, we express the drag in the standard form

$$P_{\mathrm{drag}} = -\frac{1}{2} \cdot \rho_1 \cdot v^2, \tag{6}$$

where $\rho_1 = 1.4 \cdot m_{\mathrm{H}} \cdot n_{\mathrm{halo}}$ is the density of the halo gas and $v = 220\,\mathrm{km\,s}^{-1}$ is the space velocity of the LMC relative to the halo (Lin et al. 1995). We equate this drag pressure to the internal pressure of the gas and/or plasma at the leading edge of the LMC. Using the parameters which we derived for the plasma of the wedge, the pressure

$$P_{\mathrm{gas}} = \frac{1}{2} \cdot n_{\mathrm{wedge}} \cdot \mathrm{k} \cdot T, \tag{7}$$

yields a halo density of $n_{\mathrm{halo}} \simeq 2.5 \cdot 10^{-2}\,\mathrm{cm}^{-3}$. This density is more than a factor of 10 larger than other estimates referring to about the same distance from the Galaxy. Similar arguments are being used by Weiner & Williams (1996) to explain the observed Hα emission at the leading edge of the Magellanic Stream cloud MS IV. However, the X-ray emitting plasma is quite likely not in pressure equilibrium with the surrounding medium. It may be in the state of over-pressured and thus still expanding.

The agreement of the X-ray absorbing column densities with the ones derived from *IRAS* 100 μm dust emission indicates that the X-ray emitting plasma is located at, or close to, the far side of the neutral gas distribution of the LMC. This information on the 3-D structure of the LMC is confirmed by the properties of a giant polarized radio continuum loop emerging out of the plane of the LMC (Klein et al. 1993). At 6.3 cm this loop subtends the full extent of our X-ray shadow, and the most strongly polarized regions coincide with the deep parts of the X-ray shadow. Apparently, the magnetic loop commences in the far side of the LMC – possibly within the X-ray emitting region that we called wedge. Klein et al. (1993) find that the loop stretches between the main disk of the LMC and the so called L-component of the H I gas in the LMC (Luks & Rohlfs 1992). The loop then emerges from the ISM of the LMC towards the side facing our Galaxy at the western boundary of the X-ray dark molecular cloud. This cloud appears to have the radial velocities which also characterize the L-component.

In this picture, the X-ray dark molecular cloud – as well as the L-component – are expanding away from the disk of the LMC towards the Galaxy. The disruption that has caused this material to separate from the disk is certainly related to the giant loop that is observed in the polarized radio continuum. Possible sources of this disruption are supernova events or ram-pressure processes occuring during the orbit of the LMC around the Galaxy.

Of course, the scenario sketched here is only a first attempt towards a 3-D picture of the LMC and the numbers need to be verified by improved data and other methods. However, the qualitative picture is certainly viable, and the determination of the differential 3-D structure of X-ray absorbing and emitting layers in the LMC and their relation to other features like the

giant polarized radio continuum loop to the south-west of 30 Dor demonstrate the potential of analyzing X-ray data of extended extragalactic sources.

References

Blondiau M.J., 1996, Ph. D. thesis, Univ. of Bonn, in prep.
Cohen R.S., Dame T.M., Garay G., Montani J., Rubio M., Thaddeus P., 1988, ApJ 331, L95
Hasinger G., Burg R., Giacconi R., Hartner G., Schmidt M., Trümper J., Zamorani G., 1993, A&A 275, 1
Herbstmeier U., Heithausen A., Mebold U., 1993, A&A 272, 514
Johansson L.E.B., Olofsson H., Hjalmarson Å., Gredel R., Black J.H., 1994, A&A 291, 89
Kerp J. 1994, A&A 289, 597
Haynes R.F., Klein U., Wayte S. et al., 1993, A&A 271, 402
Kampmann H., 1996, Ph. D. thesis, Univ. of Bochum, in prep.
Klein U., Haynes R.F., Wielebinski R., Meinert D., 1993, A&A 271, 402
Kutner M.L., 1996, IAU Symposium 170, in press
Lin D.N.C., Jones B.F., Klemola A.R., 1995, ApJ 439, 652
Luks Th., Rohlfs K., 1992, A&A 263, 41
Morrison R., McCammon D., 1983, ApJ 270, 119
Osterberg J., 1996, Ph. D. thesis, Univ. of Bonn, in prep.
Pfeffermann E., Briel U.G., Hippmann H. et al., 1986, in Proc of SPIE 733, 519
Plucinsky P.P., Snowden S.L., Briel U.G., Hasinger G., Pfeffermann E., 1993, ApJ 418, 519
Raymond J.C., Smith B.W., 1977, ApJS 35, 419
Schwering P., 1988, Ph. D. thesis, Univ. of Leiden
Snowden S.L., Cox D., McCammon D., Sanders W.T., 1990, ApJ 364, 118
Snowden S.L., Freyberg M.J., 1993, ApJ 404, 403
Snowden S.L., McCammon D., Verter F., 1993, ApJ 409, L21
Snowden S.L., McCammon D., Burrows D.N., Mendenhall J.A., 1994, ApJ 424, 714
Snowden S.L., Petre R., 1994, ApJ 436, L123
Trümper J., 1983, Adv. of Space Res. 2(4), 241
Trümper J., Hasinger G., Aschenbach G., Braeuninger H., Briel U.G., 1991, Nat 349, 579
Wang Q., Hamilton T., Helfand D.J., Wu, X., 1991, ApJ 374, 475
Weiner B.J., Williams T.B., 1996, AJ 111, 1156
Westerlund B.E., 1990, A&AR 2, 29